

Multiscale AM-FM Demodulation and Image Reconstruction Methods With Improved Accuracy

Víctor Murray, *Member, IEEE*, Paul Rodríguez, and Marios S. Pattichis, *Senior Member, IEEE*

Abstract—We develop new multiscale amplitude-modulation frequency-modulation (AM-FM) demodulation methods for image processing.¹ The approach is based on three basic ideas: i) AM-FM demodulation using a new multiscale filterbank, ii) new, accurate methods for instantaneous frequency (IF) estimation, and iii) multiscale least squares AM-FM reconstructions. In particular, we introduce a variable-spacing local linear phase (VS-LLP) method for improved instantaneous frequency (IF) estimation and compare it to an extended quasilocal method and the quasi-eigen function approximation (QEA). It turns out that the new VS-LLP method is a generalization of the QEA method where we choose the best integer spacing between the samples to adapt as a function of frequency. We also introduce a new quasi-local method (QLM) for IF and IA estimation and discuss some of its advantages and limitations. The new IF estimation methods lead to significantly improved estimates. We present different multiscale decompositions to show that the proposed methods can be used to reconstruct and analyze general images.

Index Terms—Amplitude-modulation frequency-modulation (AM-FM), image demodulation, multiscale image analysis.

I. INTRODUCTION

THE development of accurate methods for estimating amplitude-modulation frequency-modulation (AM-FM) image decompositions is of great interest due to its potentially significant impact on image analysis applications (see recent examples by Pattichis and Bovik in [1], Kokkinos *et al.* [2]). In this paper, we consider methods that lead to accurate AM-FM estimates and general image reconstructions. We focus our attention on AM-FM components estimated over a multiscale filterbank and demonstrate that this restriction allows us to reconstruct general images.

A general AM-FM representation model approximates images using a sum of AM-FM components as given by

$$I(x, y) \approx \sum_{n=1}^M a_n(x, y) \cos \varphi_n(x, y). \quad (1)$$

Manuscript received October 10, 2008; revised December 08, 2009. First published January 12, 2010; current version published April 16, 2010. This work was supported by the Air Force Research Laboratory under grant number QA9453-06-C-0211. The associate editor coordinating the review of this manuscript and approving it for publication was Dr. Eero P. Simoncelli.

V. Murray and M. S. Pattichis are with the Image and Video Processing and Communications Lab (ivPCL), Department of Electrical Engineering and Computer Engineering, University of New Mexico, Albuquerque, NM 87131 USA (e-mail: vmurray@ieee.org; pattichis@ece.unm.edu).

P. Rodríguez is with the Digital Signal Processing Group at the Pontifical Catholic University of Peru, Lima, Peru (e-mail: prodrig@pucp.edu.pe).

Digital Object Identifier 10.1109/TIP.2010.2040446

¹There is currently a patent pending that covers the AM-FM methods and applications described in this paper.

In (1), a continuous image $I(\cdot)$ is a function of a vector of spatial coordinates (x, y) . A collection of M different components are used to model essential image modulation structure. The amplitude functions $a_n(x, y)$ are always assumed to be non-negative. In the context of this paper, we will consider the cases when $M = 2$ (single scale) to 4 (three scales), and $M = 5$ (AM-FM harmonics).

Nonstationary images are represented using AM-FM in terms of amplitude and phase functions. The basic idea is to let the frequency-modulated (FM) components $\cos \varphi_n(x, y)$ capture fast-changing spatial variability in the image intensity. For each phase function $\varphi_n(x, y)$ we define the instantaneous frequency (IF) $\nabla \varphi_n(x, y)$ in terms of the gradient

$$\nabla \varphi_n(x, y) = \left(\frac{\partial \varphi_n}{\partial x}(x, y), \frac{\partial \varphi_n}{\partial y}(x, y) \right). \quad (2)$$

There is strong interest in the further development of AM-FM models due to the wide range of applications in various areas in signal, image and video processing. In what follows, we provide a partial list. Early work in speech signal analysis was reported by Kaiser *et al.* in [3]–[5]. Performance in noise was reported by Bovik *et al.* in [6]. Girolami and Vakman developed the Quasi Local Method in [7]. Applications in 1-D signals have been reported by several groups [8]–[12]. Multicomponent AM-FM analysis for 1-D signals and speech processing have been reported by Maragos and his collaborators in [8] and [13]–[15], as well as by other groups in [16] and [17].

There are several AM-FM applications in image processing. For image analysis, we mention shape from shading by Super and Bovik in [18], fingerprint classification by Pattichis *et al.* [19], image retrieval in digital libraries by Havlicek *et al.* in [20] and general applications in image segmentation by Pattichis *et al.* and collaborators in [21]–[23]. Pattichis and Bovik provided a general theoretical framework for FM applications in [1]. Acton, Havlicek, and collaborators described an application in image inpainting in [24] and a somewhat related application in repairing damaged image textures in [25]. In video image analysis, Rodríguez *et al.* [26] described an application in cardiac (Motion-mode ultrasound) image segmentation. In earlier work, Fleet and Jepson developed phase-based methods for motion estimation in [27]. In related and more recent work, we demonstrated new methods for motion estimation and reconstruction in [28] and [29].

There has also been significant research on the use of AM-FM components to reconstruct digital images. Pattichis *et al.* developed a general theory for computing optimal, multidimensional FM transforms for general images in [30]. General multicomponent AM-FM component tracking has also been studied by

Havlicek and collaborators in [31]–[34]. Furthermore, AM-FM reconstruction methods have been reported by Murray, Pattichis, Havlicek and others in [34]–[39].

Analytic image methods for AM-FM demodulation are based on extending the notion of the 1-D analytic signal to 2-D or simply to provide a Hilbert-based extension of the 1-D Hilbert-based demodulation approach. Early work can be found in Havlicek’s dissertation [40]. Larkin *et al.* [41], [42] introduced the phase quadrature transform for extending the Hilbert transform into two dimensions. Felsberg and Sommer introduced the monogenic signal, a nice extension of the analytic signal to images in [43]. Some related work on image demodulation based on the analytic image has been reported by Hahn *et al.* and collaborators in [43]–[46]. Here, the Hilbert-based approach provides a unique AM-FM demodulation method that satisfies certain conditions. As discussed by Havlicek in [40] and Vakman in [47], the proposed approach satisfies conditions on i) amplitude continuity and differentiability, ii) phase independence of scaling and homogeneity, and iii) harmonic correspondence.

Vakman provides a recent treatment of Hilbert-based methods for 1-D AM-FM signals in his book [48]. Havlicek *et al.* provide a tutorial introduction to multidimensional AM-FM demodulation techniques in [49]. Pattichis *et al.* provide an overview of advances made in the area of multidimensional AM-FM models and methods in [50].

In this paper, we will only consider multiscale AM-FM representations. Here, we approximate general images using (1) where $n = 1, 2, \dots, M$ denote AM-FM components from different scales. We use the term *scale* to refer to a collection of low, medium and high frequency components as detailed in Section III (also see Fig. 2). The proposed multiscale approach is a special case of the general multicomponent approach, in the sense that i) the AM-FM scale components are not allowed to overlap in the spectral domain and ii) each component is further restricted to specific pass-bands.

We employ several new techniques to improve the accuracy of our estimates. To improve IA estimation, we propose the use of optimally designed (in the min-max sense) digital filters. The optimally designed digital filters allow us to control the pass-band gain to be close to 1 while reducing the stop-band gain to be closer to 0. As a result, the use of digital filters allows us to remove the IA correction step that uses estimates of the IF to correct for the Gabor filterbank response (see [25]). Also, for AM-FM components falling within the desired pass-band, each digital filter will provide better IA estimates. Interference from the stop-band can be effectively controlled by keeping the stop-band gain very low.

To improve estimation accuracy, we study the use of the condition number of the underlying numerical operations. Here, for robust estimation, we require that our mathematical operations maintain low condition numbers. In this nonparametric approach, we improve IF estimation by selecting the method with the lowest condition number at each pixel. We also develop a second robust AM-FM demodulation approach, based on prior work developed by Girolami and Vakman [7] for estimating multidimensional components over the entire frequency spectrum.

Recently, Kokkinos *et al.* demonstrated a related accurate demodulation method using energy operators [2]. Here, the basic idea is to compute all necessary derivatives by convolving with derivatives of Gabor filters, as opposed to using finite differences. Kokkinos *et al.* [2] also demonstrate fast implementations of their approach by implementing the derivatives using multiplication in the frequency domain. The IA estimates are also corrected by dividing by the magnitude response of the Gabor filter at the estimated IF (see [2] for details).

We investigate the use of a small number of AM-FM components for reconstructing general input images. Here, we extract AM-FM components using dominant component analysis applied to different scales. We use robust least-squares to combine the AM-FM components. The use of robust least-squares methods provides for a correction method, where we estimate the coefficients for the AM-FM components so as to reduce interference among them. This least-squares approach had not been previously considered, possibly due to the fact that AM-FM components come from different passband filters. However, this prior approach is insufficient since it is clear that sharp changes in instantaneous frequency content can generate strong frequency components throughout the spectrum (also see Gaussian process example by Storm [51]).

In Section II, we present the foundations of AM-FM demodulation theory. In Section III, we present a mathematical analysis for the development of robust methods based on the condition number of the used functions and a multigrid approach for instantaneous frequency estimation. Then, we include robust multiscale reconstructions, using least-square methods, of the images and the design of efficient 2-D multiscale filterbanks. Section IV presents results in the sense of analysis of images and in terms of reconstruction. Two different types of input images were used: synthetic images and natural images. We discuss the results in Section V. Conclusions and future work are presented in Section VI.

II. BACKGROUND

We consider two methods for AM-FM demodulation [7], [52]. An advantage of these methods is that they operate with sums and products of four local image samples. For the Quasi-Eigenfunction Approximation (QEA) methods we work with sums and differences of pairs of image samples. For the 1-D Quasi-local method (QLM), we work with products of pairs of image samples. In this sense, the methods appear to cover quite distinct approaches to the image demodulation problem.

A. AM-FM Demodulation Methods Based on the Quasi-Eigenfunction Approximation

1) *Continuous Space AM-FM Demodulation Based on Extensions of the 1-D Analytic Signal:* First, we compute the 2-D extended analytic signal associated with $I(x, y)$. The 2-D extended analytic signal is computed using [40]

$$I_{AS}(x, y) = I(x, y) + j\mathcal{H}_{2d}[I(x, y)] \quad (3)$$

where \mathcal{H}_{2d} denotes a 2-D extension of the 1-D Hilbert transform operator. The 2-D operator is defined in terms of the 1-D

operator, operating in either the x or the y direction (see partial Hilbert transform definition in [53])

$$\mathcal{H}_{2d}[I(x, y)] = \frac{1}{\pi x} * I(x, y). \quad (4)$$

For the algorithm to work, we must have that (see [54] for the 1-D case)

$$I_{AS}(x, y) \approx a(x, y) \exp(j\varphi(x, y)). \quad (5)$$

When the approximation holds, it is possible to estimate the amplitude, the phase and the instantaneous frequency using

$$a(x, y) = |I_{AS}(x, y)| \quad (6)$$

$$\varphi(x, y) = \arctan\left(\frac{\text{imag}(I_{AS}(x, y))}{\text{real}(I_{AS}(x, y))}\right) \quad (7)$$

and

$$\omega(x, y) = \text{real}\left[-j \frac{\nabla I_{AS}(x, y)}{I_{AS}(x, y)}\right]. \quad (8)$$

Here, we note that amplitude and phase estimates are trivially derived from (5). The IF estimate given in (8) can be verified by a direct substitution of (5) into (8). For estimating the discrete-space version of the extended analytic signal of (3), we use a 2-D FFT (see [40] for details).

2) *Quasi-Eigenfunction Approximation Algorithm (QEA)*: For developing the algorithm, we assume that ideal samples of the continuous-space image are available to us. We will not address sampling issues associated with this assumption (we of-course do require $I(\cdot)$ to be bandlimited). We write

$$I(k_1, k_2) = a(k_1, k_2) \cos \varphi(k_1, k_2) \quad (9)$$

where k_1 and k_2 assume integer values of the continuous-space arguments x and y . Thus, in what follows, we will interpret $I(k_1, k_2)$ as a continuous-space real-valued function. We compute the 2-D-extended analytic signal $\hat{I}_{AS}(k_1, k_2)$ using the partial Hilbert Transform [53], implemented using the fast Fourier transform (FFT). The instantaneous frequency can be estimated using inverse trigonometric functions (see [52]). In our discussion of the variable spacing linear phase model we will derive the same inverse trigonometric function expressions. We will thus not repeat them here. The IA and IP are estimated using $\hat{I}_{AS}(k_1, k_2)$ as described in (6) and (7).

B. Quasi-Local Method (QLM)

The Quasi-Local Method (QLM) was introduced, for 1-D signals and half the discrete frequency spectrum, by Girolami and Vakman in [7]. Consider the continuous-space signal $f(k_1, k_2) = a(k_1, k_2) \cos \varphi(k_1, k_2)$, ideally sampled at the integers. Also, consider the lowpass filter $h_{LP}(k_1, k_2)$.

Define $g_{(\epsilon_1, \epsilon_2)_x}(k_1, k_2) = f(k_1 + \epsilon_1, k_2) f(k_1 - \epsilon_2, k_2)$ and $g_{(\epsilon_1, \epsilon_2)_y}(k_1, k_2) = f(k_1, k_2 + \epsilon_1) f(k_1, k_2 - \epsilon_2)$ where $\epsilon_1, \epsilon_2 \geq 0$ and note that

$$\begin{aligned} g_{(\epsilon_1, \epsilon_2)_x}(k_1, k_2) &= \frac{a_{(\epsilon_1, \epsilon_2)_x}(k_1, k_2)}{2} \\ &\times [\cos((\epsilon_1 + \epsilon_2)\omega_{(\epsilon_1, \epsilon_2)_x}(k_1, k_2)) \\ &+ \cos(\varphi(k_1 + \epsilon_1, k_2) \\ &+ \varphi(k_1 - \epsilon_2, k_2))] \end{aligned} \quad (10)$$

where

$$a_{(\epsilon_1, \epsilon_2)_x}(k_1, k_2) = a(k_1 + \epsilon_1, k_2) a(k_1 - \epsilon_2, k_2)$$

and

$$\omega_{(\epsilon_1, \epsilon_2)_x}(k_1, k_2) = (\varphi(k_1 + \epsilon_1, k_2) - \varphi(k_1 - \epsilon_2, k_2)) / (\epsilon_1 + \epsilon_2).$$

In what follows, we will consider the cases for $\epsilon_1 = 0, 1$ and $\epsilon_2 = 0, 1$. First, we define

$$\check{g}_{(\epsilon_1, \epsilon_2)}(k_1, k_2) = h_{LP}(k_1, k_2) * g_{(\epsilon_1, \epsilon_2)_x}(k_1, k_2). \quad (11)$$

Here, for $(\epsilon_1, \epsilon_2) = (0, 0)$, we note that $g_{(0,0)_x} = g_{(0,0)_y}$. In this special case, we drop subscripts and simply use $g_{(0,0)}$ to estimate the IA using

$$\hat{a}(k_1, k_2) = \sqrt{2\check{g}_{(0,0)}(k_1, k_2)}. \quad (12)$$

For the x -component of the IF, we get

$$\begin{aligned} \frac{\partial \varphi}{\partial x}(k_1, k_2) \\ = \arccos\left(\frac{R_1(k_1, k_2) + \sqrt{R_1^2(k_1, k_2) + 8}}{4}\right) \end{aligned} \quad (13)$$

where

$$R_1(k_1, k_2) = \frac{2\check{g}_{(1,1)_x}(k_1, k_2)}{\check{g}_{(1,0)_x}(k_1, k_2) + \check{g}_{(0,1)_x}(k_1, k_2)}. \quad (14)$$

Similar analysis is done for the y direction. In order to avoid aliasing, the IF of the input signal must be restricted to $0 < \partial\varphi/\partial x < \pi f_s/2$, for the x -direction, where f_s is the sampling frequency. A similar condition is required for the y -direction. In [7] it is proposed to either resample or oversample the input signal with a higher f_s in order to overcome this restriction.

III. METHODS

Given the input image I , we first apply the partial Hilbert transform (4) to form a 2-D extension of the 1-D analytic signal: I_{AS} . I_{AS} is processed through a collection of bandpass filters as is showed in Fig. 1. Each processing block will produce the instantaneous amplitude, the instantaneous phase, and the instantaneous frequencies in both x and y directions by means of either the QEA method (Section II-A2) or the QLM method (Section III-B3). As discussed in the caption of Fig. 1, the basic idea is to apply *dominant component analysis* over each scale. The approach produces a single AM-FM component from each scale. The algorithm adaptively selects the estimates from the bandpass filter with the maximum response. This approach does not assume spatial continuity and allows the model to quickly adapt to singularities in the image. The performance of the AM-FM demodulation algorithm in one and two-dimensions has been extensively studied (see [40]).

A. 2-D Filterbank Design for Applications in Discrete Images

We use separable multiscale filterbanks covering the whole frequency spectrum (see Fig. 2). For real-valued bandpass filters, each separable channel filter has support over four quadrants. Here, to maintain support over only two quadrants, we use FFT prefiltering to remove support in two quadrants (either

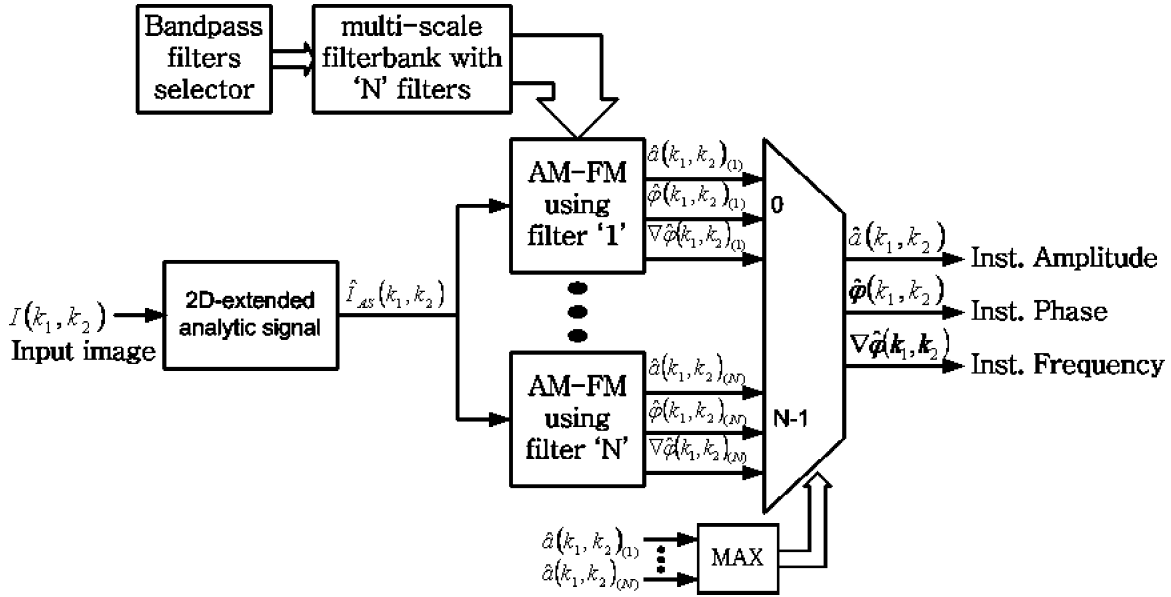


Fig. 1. Multiscale AM-FM demodulation. In this figure, we are only showing how we estimate a single AM-FM component from a single scale. Here, we define “scale” as a collection of bandpass filters, categorized into low/medium/high based on frequency magnitude. For each scale, the corresponding collection of filters is listed in Table II. The spectral support of these filters is shown in Fig. 2. The bandpass filter selector (upper left) is used to define the bandpass filters that correspond to each scale. At each pixel, we examine the IA estimates from each channel filter. We then select the channel estimates that produces the largest IA estimate. The collection of all estimates from all pixels is then used to form the dominant component for the scale. This method is a direct extension of the standard dominant component analysis [40].

the two left or right quadrants, as needed, also see the partial Hilbert transform discussion in Section II-A1). Here, we note that in the full system implementation, the extended analytic signal will only have support in the lower two quadrants. Thus, in effect, each channel filter operates over a single quadrant. The filters were designed using an optimal min-max, equiripple approach. Passband ripple was set at 0.017 dB and the stopband attenuation was set to 66.02 dB. For the transition bandwidth, we require that i) it remains lower than the passband bandwidth, and that ii) it remains sufficiently large so that the passband and stopband requirements can be met with a reasonable number of digital filtering coefficients. Here, we note that the transition widths are relatively less important for the high frequencies, since they also come with filters of larger passband bandwidths. On the other hand, low-frequencies require relatively larger transition widths (from stopband to passband) since images contain larger, low-frequency components and the transitions occur over smaller passbands. We fixed the transition bandwidths to $\pi/10$, a choice that provided a reasonable solution for meeting these requirements. Based on this approach, the unit gain over the passband eliminated the need for amplitude correction, as required by a Gabor filterbank approach (see [52]).

B. Robust Discrete Image AM-FM Demodulation Methods

We develop robust AM-FM demodulation methods. We begin with a discussion on the stable evaluation of functions in Section III-B1, and extend it to the stable evaluation of inverse trigonometric functions in Section III-B2. An extension to the Quasi-local method is given in Section III-B3. In Section III-B4, we present a new and robust method for the IF estimation: a variable spacing, local linear phase (VS-LLP) method.

1) *Numerically Stable Evaluation of Functions*: In order to develop robust demodulation techniques, we need to ensure that no intermediate computation step results in the loss of significance [55], [56]. We are particularly interested in avoiding excessive relative error.

First, consider the Taylor theorem with remainder $f(x+h) = f(x) + hf'(x) + R(x)$, where $|R(x)| \leq \max_{t \in [x, x+h]} |f''(t)| h^2/2$. We have that the relative perturbation is given by [56]

$$\frac{f(x+h) - f(x)}{f(x)} \approx \frac{hf'(x)}{f(x)} = \left[\frac{xf'(x)}{f(x)} \right] \frac{h}{x}, x \neq 0. \quad (15)$$

The error in the relative error approximation is bounded by $R(x)/f(x) \leq h^2/(2f(x)) \max_{t \in [x, x+h]} |f''(t)|$.

In (15), we note that the relative perturbation in x (given by h/x) is amplified by the condition number given by

$$(\text{cond } f)(x) := \left| \frac{x \cdot f'(x)}{f(x)} \right|. \quad (16)$$

More generally, in evaluating functions, we need to consider the condition numbers of all intermediate functions used in the computation. The computation is unstable and prone to error if any one intermediate function has a large condition number. Here, we want to select the demodulation estimate with the minimum possible condition number [55]. This is the basic idea behind the VS-LLP method (see Section III-B4).

2) *Numerically Stable Evaluation of Inverse Trigonometric Functions*: In our development of AM-FM demodulation methods, we have encountered three inverse trigonometric

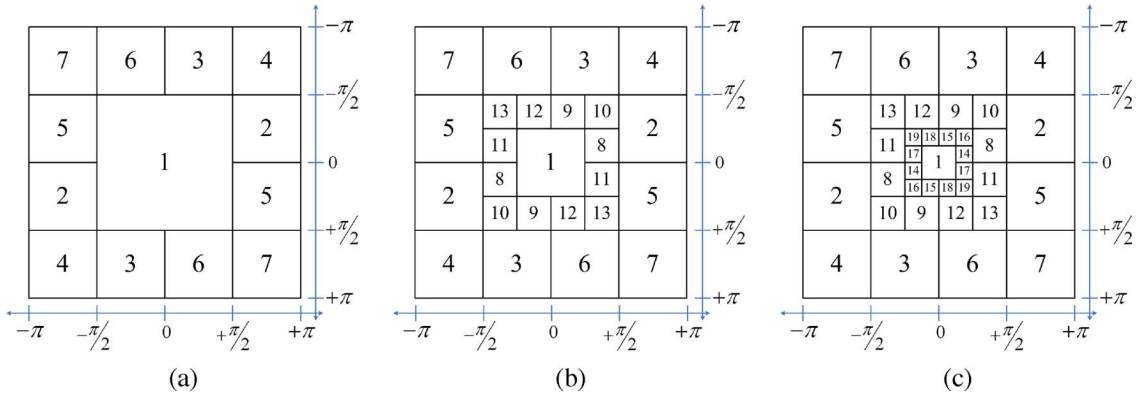


Fig. 2. Spectral supports of the channel filters used for multiscale analysis (see Section III-A). We present the channel filters for (a) single-scale, (b) two-scale, and (c) three-scale filterbanks. We refer to Table II for the channel filters that correspond to each scale.

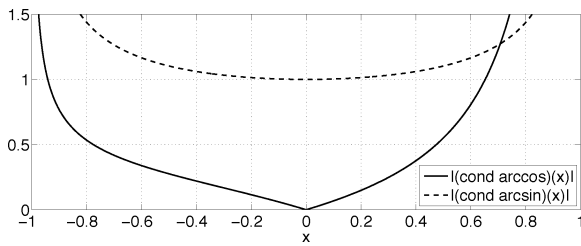


Fig. 3. Absolute value of the condition number for the arccos (solid line) and arcsin (dash line) is shown. From this graph, it is clear that we have the most stable evaluation for the arccos function for $|x| \approx 0$.

functions: arcsin, arccos, and arctan. Their condition numbers are given by

$$(\text{cond arccos})(x) = \frac{|x|}{|\arccos(x)|\sqrt{1-x^2}} \quad (17)$$

$$(\text{cond arcsin})(x) = \frac{|x|}{|\arcsin(x)|\sqrt{1-x^2}} \quad (18)$$

and

$$(\text{cond arctan})(x) = \frac{|x|}{|\arctan(x)||1+x^2|}. \quad (19)$$

For the arccos, it is interesting to note that the approximation error remains low around $x = 0$. We note that the condition numbers become infinite for both the arcsin and the arccos for $x = \pm 1$ (see Fig. 3). Otherwise, we have finite condition numbers for all values of x , including the cases when $\arcsin(x) = 0$, $\arccos(x) = 0$, or $\arctan(x) = 0$.

Note from Fig. 3 that for $|x| < 0.6$ evaluating the arccos is more stable than evaluating the arcsin. Furthermore, the most stable evaluations occur for small values of $|x|$, when using the arccos function.

Even though the arccos function provides the most stable evaluations, we also need to use the arcsin function to estimate the proper IF quadrant. On the other hand, we also find that there are also significant problems in accurate estimation at very high frequencies.

3) *Extended IF Estimation Using the Quasi-Local Method:* For the quasi-local method presented in Section II-B, the IF is limited between 0 and $\pi/2$. In this Section, we extend the QLM method for estimating the IF over the entire range of possible

values. We begin with a discussion of the 1-D case. To develop a corrected model, we replace $\omega(k)$ by $\xi(k) = \pi - \omega(k)$ in the derivations summarized in Section II-B. This yields the modified expressions

$$\xi(k) = \arccos\left(\frac{-R(k) + \sqrt{R^2(k) + 8}}{4}\right) \quad \text{and} \quad (20)$$

$$\omega(k) = \pi - \xi(k). \quad (21)$$

which can be used when the IF is restricted between $\pi/2$ and π .

For estimating the IF over the entire range of values, we use two digital filters to allow for estimation over two disjoint bands: $[0, \pi/2]$ and $[\pi/2, \pi]$. The input signal is filtered using a low-pass filter with a passband of $[-\pi/2, \pi/2]$ and a bandpass filter with a passband of $[-\pi, -\pi/2] \cup [\pi/2, \pi]$. Over the passband of the lowpass filter, we estimate IFs restricted to the range of $[0, \pi/2]$. Over the passband of the bandpass filter, we estimate IFs restricted to the range of $[\pi/2, \pi]$.

Since prior to the estimation of the IF, we have no knowledge where the IF is, we use the instantaneous amplitude to decide which estimate to use. We compute an IA estimate from the lowpass filter and a second IA estimate from the bandpass filter. We then select the AM-FM estimates from the filter that gave the largest IA estimate (as in dominant component analysis).

We return to (10), and analyze the error in the approach. The basic idea in this algorithm is that the lowpass filter of (11) should select the first term in (10), while rejecting the second term.

For 2-D signals, we have that

$$\widehat{\frac{\partial \varphi}{\partial x}}(k_1, k_2) = \pi - \arccos\left(\frac{-R_1(k_1, k_2) + \sqrt{R_1^2(k_1, k_2) + 8}}{4}\right) \quad (22)$$

$$\text{and} \quad \widehat{\frac{\partial \varphi}{\partial y}}(k_1, k_2) = \pi$$

$$- \arccos\left(\frac{-R_2(k_1, k_2) + \sqrt{R_2^2(k_1, k_2) + 8}}{4}\right) \quad (23)$$

when $\pi/2 \leq \partial \varphi / \partial x < \pi$ and $\pi/2 \leq \partial \varphi / \partial y < \pi$, respectively.

4) *A Robust Instantaneous Frequency Estimation Based on a Local Linear Phase (LLP) Model:* We present a new method for robust IF estimation based on a local linear phase model [1]. We use the term variable spacing, local linear phase methods (VS-LLP) to describe the approach we develop in this section.

In the original QEA, the IF estimate was used to correct the instantaneous amplitude estimate due to prefiltering by a Gabor filterbank (with nonunit gain over the passband, see [40] and [52]). In our proposed approach, due to the unit gain over the passbands, we can use a plug-in rule to produce a new signal \bar{I}_{AS} with unit instantaneous amplitude using

$$\begin{aligned}\bar{I}_{AS}(k_1, k_2) &= \frac{\hat{I}_{AS}(k_1, k_2)}{|\hat{I}_{AS}(k_1, k_2)|} \\ &= \frac{a(k_1, k_2) \exp(j\hat{\varphi}(k_1, k_2))}{a(k_1, k_2)} \\ &= \exp(j\hat{\varphi}(k_1, k_2)).\end{aligned}\quad (24)$$

Let us consider a linear approximation for the estimated phase $\hat{\varphi}(p_1, p_2)$ of order $\| [p_1 - k_1, p_2 - k_2] \|^2$, given by $\hat{\varphi}(p_1, p_2) \approx \hat{\varphi}(k_1, k_2) + [p_1 - k_1, p_2 - k_2] \nabla \hat{\varphi}(k_1, k_2)$. Then, we get

$$\begin{aligned}& \frac{\bar{I}_{AS}(k_1 + n_1, k_2) + \bar{I}_{AS}(k_1 - n_1, k_2)}{2\bar{I}_{AS}(k_1, k_2)} \\ &= \frac{\exp(j\hat{\varphi}(k_1 + n_1, k_2)) + \exp(j\hat{\varphi}(k_1 - n_1, k_2))}{2 \exp(j\hat{\varphi}(k_1, k_2))} \\ &\approx \frac{\exp(j\hat{\varphi}(k_1, k_2)) [\exp(jn_1 \nabla \hat{\varphi}) + \exp(-jn_1 \nabla \hat{\varphi})]}{2 \exp(j\hat{\varphi}(k_1, k_2))} \\ &= \cos \left(n_1 \frac{\partial \varphi}{\partial x}(k_1, k_2) \right).\end{aligned}\quad (25)$$

This gives an arc-cosine expression for estimating the instantaneous frequency component using

$$\begin{aligned}& \widehat{\frac{\partial \varphi}{\partial x}}(k_1, k_2) \\ &= \frac{1}{n_1} \arccos \left(\frac{\bar{I}_{AS}(k_1 + n_1, k_2) + \bar{I}_{AS}(k_1 - n_1, k_2)}{2\bar{I}_{AS}(k_1, k_2)} \right).\end{aligned}\quad (26)$$

The analysis for $\widehat{\frac{\partial \varphi}{\partial y}}$ is similar. Here, we note that (26) is in agreement with the QEA as presented in [52].

For low IF magnitude, it is clear that the local linear phase approximation will hold over a larger range of n_1, n_2 . For larger IF magnitude, we will need to modulate the phase down to lower frequencies, as we discuss in Section III-B5.

The expression in (26) requires that we evaluate the arc-cosine function at different possible values for n_1 . For stable function evaluations, we consider the argument to the arc-cosine function $\gamma_{\arccos}(n_1) = (\bar{I}_{AS}(k_1 + n_1, k_2) + \bar{I}_{AS}(k_1 - n_1, k_2)) / 2\bar{I}_{AS}(k_1, k_2)$.

Here, our goal is to consider integer values for n_1 for which we want to have $\gamma_{\arccos}(n_1)$ to be as close to 0 as possible (see Fig. 3). We consider four possible values: $n_1 = 1, 2, 3$ and 4. We do not increase more the value of n_1 since the condition number can then become unstable (see (17) and Fig. 3).

To establish the limits of our approach, we begin by noting that for the argument of the $\gamma_{\arccos}(\cdot)$ to be zero, we require that

$$\bar{I}_{AS}(k_1 - n_1, k_2) = -\bar{I}_{AS}(k_1 + n_1, k_2).$$

Thus, for $n_1 = 1$, the maximum frequency that we can attain, without requiring interpolation, will be $w_1 = \pi/2$. However, we get around this limitation by modulating the input image to lower frequencies. On the other hand, for the maximum value of $n_1 = 4$, we can consider IF estimation down to $w_1 = \pi/8$.

To further improve the accuracy of the approach, please recall that the AM-FM demodulation algorithm is applied over a filterbank of bandpass filters (see Fig. 4). Clearly, it is possible for the actual IF to fall outside of the spectral support of any given channel filter. Given that the filterbank provides coverage of the discrete frequency plane and that the components of natural images of practical interest are expected to be locally coherent almost everywhere [57], in what follows we will assume that it is sufficient to consider that the IF falls locally within the passband of the dominant channel filter almost everywhere. This will clearly not always be the case. We refer the reader to [54] for the relationship between the IF and the Spectrum of a signal. Here, our approach is to look for the minimum arc-cosine argument that also falls within the passband of the estimating bandpass filter. We thus compute

$$\min_{n_1=1,2,3,4} |\gamma_{\arccos}(n_1)| \quad \text{subject to} \quad \widehat{\frac{\partial \varphi}{\partial x}} \in [w_{p_{1x}}, w_{p_{2x}}] \quad (27)$$

where $[w_{p_{1x}}, w_{p_{2x}}]$ denotes the passband for the horizontal frequencies. For the minimum value of $\gamma_{\arccos}(n_1)$ we evaluate (26) to determine $\widehat{\frac{\partial \varphi}{\partial x}}$. A similar approach is taken for $\widehat{\frac{\partial \varphi}{\partial y}}$.

5) *Extended LLP for High Frequencies:* From our discussion of the VS-LLP method, we recall that the method is limited to $\pi/2$. For higher frequencies we are thus led to apply modulation to the input image. Thus, for high frequencies, we multiply by $\exp(jw_{M_1}k_1 + jw_{M_2}k_2)$ to modulate the input signal to lower frequencies. The frequencies w_{M_1} and w_{M_2} are determined by the frequency support of the bandpass filter where the dominant amplitude is to be estimated. Table I shows the values of w_{M_1} and w_{M_2} depending on the frequency support of the signal.

6) *Prefiltering and Postfiltering:* For wide-band single component signals, the limited bandwidths of the channel filters can significantly reduce estimation accuracy. In this case, we apply a 3×3 median filter to the input signal. Also, the same median filter is applied to the IF estimation outputs (for both x and y directions) to provide continuity in the estimates. Prefiltering and postfiltering has also been used for multicomponent signals in [4], [5], and [52].

C. Image Reconstruction Methods

In this Section, we discuss multiscale least-squares methods for reconstructing general images. We consider three different approaches: i) using AM-FM harmonics (Section III-C1), ii) using AM-FM components extracted from different scales

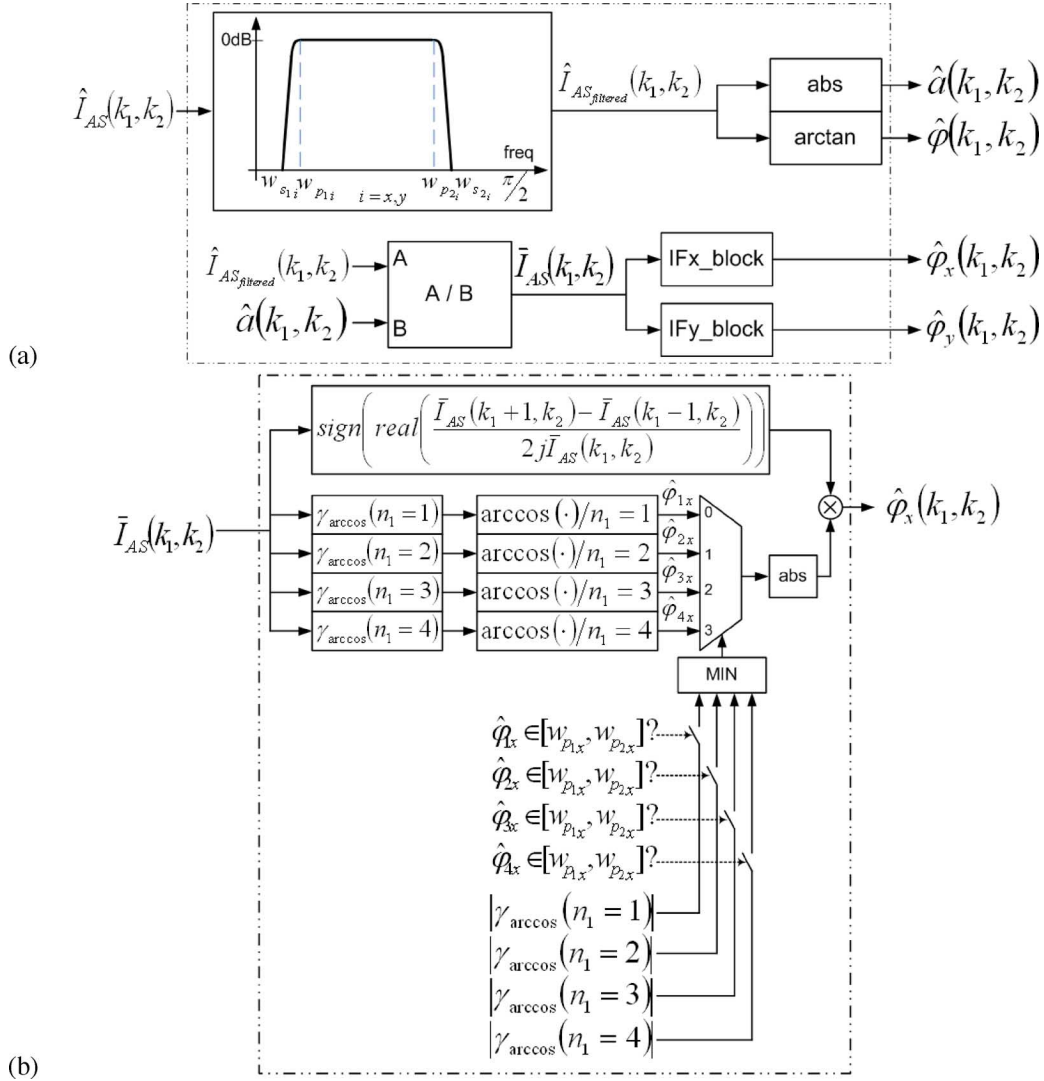


Fig. 4. VS-LLP block diagram using a single bandpass filter is shown in (a). The IFx_block is shown in (b). The IFy_block is similar. Here, $\gamma_{\arccos}(n_1) = (\bar{I}_{AS}(k_1 + n_1, k_2) + \bar{I}_{AS}(k_1 - n_1, k_2)) / (2\bar{I}_{AS}(k_1, k_2))$.

TABLE I
MODULATION FREQUENCY FACTORS FOR HIGH FREQUENCY SIGNALS. THE BANDPASS FILTER NUMBERS REFER TO FIG. 2

Bandpass filter	w_{M_1}	w_{M_2}	Bandpass filter	w_{M_1}	w_{M_2}
2	$+\pi/2$	0	3	0	$-\pi/2$
4	$+\pi/2$	$-\pi/2$	5	$-\pi/2$	0
6	0	$-\pi/2$	7	$-\pi/2$	$-\pi/2$

TABLE II
BANDPASS FILTERS CORRESPONDING TO DIFFERENT IMAGE SCALES (SEE FIG. 2)

Scale	Single-scale	Two-scale	Three-scale
LPF	1	1	1
High frequencies	2, 3, 4, 5, 6, 7	2, 3, 4, 5, 6, 7	2, 3, 4, 5, 6, 7
Medium frequencies	NA*	8, 9, 10, 11, 12, 13	8, 9, 10, 11, 12, 13
Low frequencies	NA*	NA*	14, 15, 16, 17, 18, 19

NA* = Not Applicable.

(Section III-C3), and iii) a combined approach (Section III-C2). For our reconstructions we use least squares methods derived

from the proposed multiscale decomposition that are computed using QEA estimates of the phase and instantaneous amplitude.

1) *Least-Squares Reconstructions using AM-FM harmonics (LESHA)*: We first consider reconstructing an image using its AM-FM harmonics (see [19])

$$\hat{I}(k_1, k_2) \approx d + \sum_{n=1}^h c_n a(k_1, k_2) \cos(n\varphi(k_1, k_2)). \quad (28)$$

In (28), d denotes a constant DC image. The instantaneous amplitude $a(k_1, k_2)$ and the instantaneous phase $\varphi(k_1, k_2)$ are estimated using dominant component analysis over all scales (see Fig. 2).

We then want to compute the AM-FM harmonic coefficients $c_n, n = 1, 2, \dots, h$, so that $\hat{I}(k_1, k_2)$ is a least-squares estimate of $I(k_1, k_2)$ over the space of the AM-FM harmonics. Let the column vector c_n denote the AM-FM basis coefficients that we need to estimate. Let $c_0 = d$. We estimate the coefficients in c by solving the quadratic minimization problem

$$\operatorname{argmin}_c \|b - Ac\|^2. \quad (29)$$

Here, we have that $Ac = b$ where the columns of A contain the AM-FM basis functions. Thus, the first column of A is filled with 1's, while the i th column is filled with the values of the $(i - 1)$ th AM-FM harmonic and b is a column vector of the input image. We compute c_n using

$$\begin{bmatrix} d = c_0 \\ c_1 \\ \vdots \\ c_M \end{bmatrix} = (A^T A)^{-1} (A^T b). \quad (30)$$

We also compute an orthonormal basis over the space of the AM-FM harmonics using the modified Gram-Schmidt (MGS) algorithm [58] (which can also be used to provide least squares estimates of the input image).

2) *Least-Squares Reconstructions Using AM-FM Harmonics and the LPF (LESHAL)*: We extend LESHA by simply adding the low-pass filter (LPF) output to the DC and the AM-FM harmonics. We have

$$\hat{I}(k_1, k_2) \approx d + c_0 G(k_1, k_2) + \sum_{n=1}^h c_n a(k_1, k_2) \cos(n\varphi(k_1, k_2)) \quad (31)$$

where h is the number of AM-FM harmonics, d denotes a constant DC image, $G(k_1, k_2)$ denotes the LPF output, $a \cos \varphi$ denotes the dominant AM-FM component estimated across scales and $a \cos n\varphi$ denotes the n th AM-FM harmonic. Here, we use the same image reconstruction method as for LESHA. In both cases, we note that the phase images are directly estimated. They are not reconstructed from the IF as discussed in [25]. This approach implies that the AM-FM component outputs are directly estimated from the outputs of the bandpass filters, avoiding errors from the integration of noisy estimates of the IF.

3) *Multiscale Least-Squares Reconstructions (MULTILES)*: The third method uses AM-FM estimates extracted from different scales. We describe the correspondence between scales and bandpass filters in Table II [also see Fig. 2(a)–(c)].

In this case, we consider least squares reconstructions given by

$$\hat{I}(k_1, k_2) \approx d + c_0 G(k_1, k_2) + \sum_{n=1}^s c_n a_n(k_1, k_2) \cos(\varphi_n(k_1, k_2)) \quad (32)$$

where s is the number of scales used, d is a global DC image estimate, $G(k_1, k_2)$ is the low-pass filter output, $a_1 \cos \varphi_1$ is the high-frequency scale AM-FM component, $a_2 \cos \varphi_2$ is the medium-frequency scale AM-FM component and $a_3 \cos \varphi_3$ is the low-frequency scale AM-FM component. We then compute the AM-FM multiscale coefficients $c_n, n = 0, 1, \dots, s$, so that $\hat{I}(k_1, k_2)$ is a least-squares estimate of $I(k_1, k_2)$. Here, we did not consider reconstructing the phase from the IF.

IV. RESULTS

A. Synthetic Images

1) *Gaussian Amplitude Modulated (Gaussian AM)*: We use

$$I(k_1, k_2) = 100 \exp \left[-\frac{1}{2} \alpha^2 \left(\left(\frac{k_1 + \frac{1}{2}}{\frac{N}{2}} \right)^2 + \left(\frac{k_2 + \frac{1}{2}}{\frac{N}{2}} \right)^2 \right) \right] \cos(w(k_1 + k_2)) \quad (33)$$

for $k_1, k_2 = -(N)/(2), \dots, (N)/(2) - 1$, with $N = 512, \alpha = 2.5$. Here, $\varphi_x(\cdot) = \varphi_y(\cdot) = w$, for $w = 5\pi/8$.

2) *Gaussian Amplitude Modulated-Quadratic Frequency Modulated (Gaussian AM-Quadratic FM)*: For this signal, we use

$$I(k_1, k_2) = 100 \exp \left[-\frac{1}{2} \alpha^2 \left(\left(\frac{k_1 + \frac{1}{2}}{\frac{N}{2}} \right)^2 + \left(\frac{k_2 + \frac{1}{2}}{\frac{N}{2}} \right)^2 \right) \right] \cos \varphi(k_1, k_2) \quad (34)$$

for $k_1, k_2 = -(N)/(2), \dots, (N)/(2) - 1, \alpha = 2.5$ and $N = 512$. The phase $\varphi(k_1, k_2)$ has a quadratic form $\varphi(k_1, k_2) = \alpha_1 k_1 + (\beta_1)/(2) k_1^2 + \alpha_2 k_2 + (\beta_2)/(2) k_2^2$, where $\beta_i = ((f_{B_i} - f_{A_i})/(N - 1)), \alpha_i = (\beta_i N)/(2) + f_{A_i}$, for $i = 1, 2$. Here, f_{B_i} represents the desired maximum instantaneous frequency in the i direction (x or y), and f_{A_i} represents the desired minimum instantaneous frequency. Setting f_{B_i} and f_{A_i} will produce $\varphi_x(k_1, k_2)$ and $\varphi_y(k_1, k_2)$ to be in desired ranges. Here, we will consider $\nabla \varphi(k_1, k_2): \varphi_x(k_1, k_2) \in [\pi/6, \pi/5]$ with $\varphi_y(k_1, k_2) = -\varphi_x(k_1, k_2)$.

3) *Results for Synthetic Images*: For all experiments, we add white Gaussian noise. We measure performance using the mean-squared error (MSE) and the peak signal-to-noise ratio (PSNR). For computing the PSNR in the estimates we use $20 \log_{10}(A/\sqrt{\text{MSE}})$, where $A = 100$ for the IA (maximum amplitude), and $A = \pi$ for the IF. Similarly, for our ‘‘signal plus noise’’ examples, for the signal-to-noise ratio (SNR), we use

TABLE III

ERROR IN IA ESTIMATION USING A NOISE FREE GAUSSIAN AMPLITUDE MODULATED—QUADRATIC FREQUENCY MODULATED SIGNAL WITH IF THAT GOES FROM $\pi/6$ TO $\pi/5$ RADIANS IN THE x DIRECTION, AND FROM $-\pi/5$ TO $-\pi/6$ IN THE y DIRECTION. ALL PSNR VALUES ARE IN DECIBELS

	<i>Quadrature</i> <i>No Filterbank</i>		<i>Hilbert</i> <i>No Filterbank</i>		<i>Two-scale</i>		<i>Three-scale</i>	
	MSE	PSNR	MSE	PSNR	MSE	PSNR	MSE	PSNR
QEA	6.09×10^{-30}	332.16	4.45×10^{-4}	73.51	0.035	54.60	0.033	54.86
QLM	-	-	-	-	0.048	53.20	0.066	51.79

TABLE IV

ERROR IN IF ESTIMATION USING A NOISE FREE GAUSSIAN AMPLITUDE MODULATED—QUADRATIC FREQUENCY MODULATED SIGNAL WITH IF THAT GOES FROM $\pi/6$ TO $\pi/5$ RADIANS IN THE x DIRECTION, AND FROM $-\pi/5$ TO $-\pi/6$ IN THE y DIRECTION. ALL PSNR ARE IN DECIBELS

	<i>Quadrature</i> <i>No Filterbank</i>		<i>Hilbert</i> <i>No Filterbank</i>		<i>Two-scale</i>		<i>Three-scale</i>	
	MSE	PSNR	MSE	PSNR	MSE	PSNR	MSE	PSNR
VS-LLP	6.43×10^{-16}	161.86	1.39×10^{-8}	88.51	2.45×10^{-8}	86.05	1.11×10^{-8}	89.48
QEA	1.27×10^{-8}	88.89	1.14×10^{-8}	69.39	2.34×10^{-8}	86.26	1.45×10^{-8}	88.33
QLM	-	-	-	-	1.21×10^{-4}	49.12	1.20×10^{-4}	49.16

TABLE V

ERROR IN AM-FM ESTIMATION USING REGULARIZED AM-FM DEMODULATION USING ENERGY OPERATORS AND A GABOR FILTERBANK (11 ORIENTATIONS, WITH TEN GABOR FILTERS PER ORIENTATION). THE RESULTS ARE PRESENTED FOR A GAUSSIAN AMPLITUDE MODULATED—QUADRATIC FREQUENCY MODULATED SIGNAL WITH IF THAT GOES FROM $\pi/6$ TO $\pi/5$ RADIANS IN THE x DIRECTION, AND FROM $-\pi/5$ TO $-\pi/6$ IN THE y DIRECTION. MEAN-SQUARED ERROR (MSE) AND PSNR (IN DECIBELS) VALUES ARE SHOWN

	<i>Noise free</i>		<i>SNR = 60dB</i>		<i>SNR = 40dB</i>		<i>SNR = 20dB</i>	
	MSE	PSNR	MSE	PSNR	MSE	PSNR	MSE	PSNR
IA	157.534	18.03	209.654	16.785	217.272	16.630	223.600	16.505
IF	1.99×10^{-6}	67.16	4.479×10^{-4}	43.431	2.568×10^{-2}	25.847	2.004×10^{-1}	16.924

$SNR = 20 \log_{10}(A/\sigma)$, where σ is the maximum amplitude of the Gaussian noise.

In Table III, we show the mean-squared error (MSE) and the PSNR for IA estimation when noise free signals are used. In the first column of results, we use the Quadrature version of the signals (computed as $a(k_1, k_2) \cos \varphi(k_1, k_2) + ja(k_1, k_2) \sin \varphi(k_1, k_2)$) instead of the partial Hilbert transform. Note that since VS-LLP and QEA follow the same approach in the IA estimation, their results are the same. In the next columns, we show the results when we do not use a filterbank, when using a two-scale filterbank and when using a three-scale filterbank. We also show the results using the QLM method. In Table IV, we present the corresponding results for IF estimation. For IF estimation, we only present the results in the x direction. Results for the y direction were very similar. For comparison, in Table V, we present results from the regularized demodulation algorithm based on Gabor filters (see [2]).

The implementation of the regularized demodulation algorithm is based on the Gabor filterbank used in [1] and [59]. The constant-Q Gabor filterbank uses 11 orientations, uniformly sampling the IF angle from 0 to π (see [59] for details). Since the Gabor filters cannot be assumed to be flat, we did apply IA correction based on the estimated IF. We note that filterbank provides a denser frequency sampling than presented in [2]. When the effective bandwidth of the AM-FM signal is large as com-

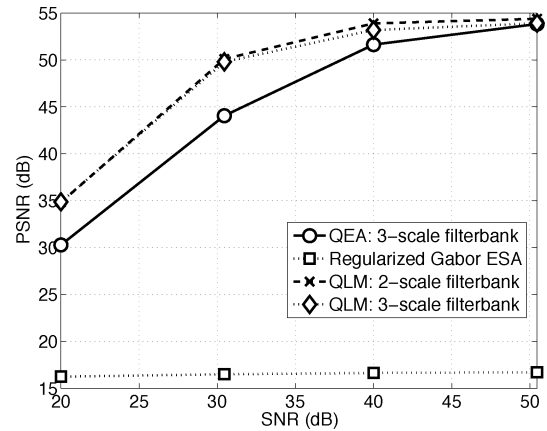


Fig. 5. PSNR for IA estimation using QEA and QLM methods with the proposed filterbanks and using regularized Gabor filters with ESA (see Table V). Please note that QEA and VS-LLP use the same method for estimating the IA. The signal used for the graphs was a Gaussian amplitude modulated—Quadratic frequency modulated signal with IF that goes from $\pi/6$ to $\pi/5$ radians in the x direction, and from $-\pi/5$ to $-\pi/6$ in the y direction (see text). QEA method plot using the three-scale filterbank (—○— line). IA estimation using Gabor filters is also shown (· · □ · · line). QLM method plots using the two-scale filterbank (— × — line) and the three-scale filterbank (· · ◇ · · line).

pared to the Gabor channel filter, we cannot correct the IA estimate based on the QEA. On the other hand, the use of more Gabor filters tends to improve the IF estimation.

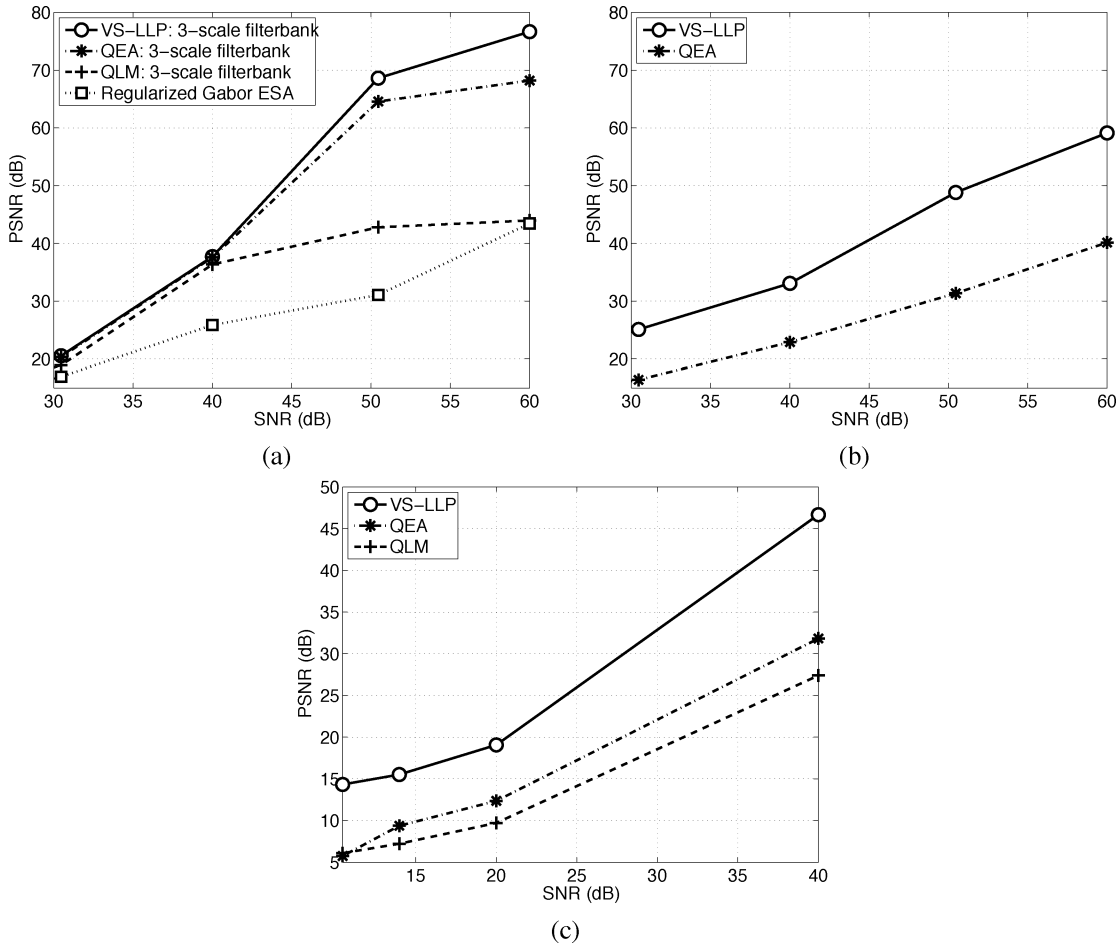


Fig. 6. PSNR plots for IF estimation. For VS-LLP, QEA, and QLM methods, we have applied pre- and postfiltering with a 3×3 median filter. For (a) and (b), we used a Gaussian amplitude modulated - Quadratic frequency modulated signal with an IF that goes from $\pi/6$ to $\pi/5$ radians in the x direction, and from $-\pi/5$ to $-\pi/6$ in the y direction. For (c), we used a Gaussian amplitude modulated with IF equal to $5\pi/8$ for both the x and y directions. We only show the results in the x direction since results in the y direction were very similar. (a) IF estimation using a three-scale filterbank for VS-LLP (-o- line), QEA (-*- line) and QLM (-+- line). We also show the results ($\cdot\cdot\cdot\Box\cdot\cdot$ line) using Gabor filters (see [2] and Table V). (b) IF estimation without using a filterbank for VS-LLP (-o- line) and QEA (-*- line). (c) IF estimation for the high frequency scale using the three-scale filterbank for VS-LLP with modulation (-o- line), QEA (-*- line) and QLM (-+- line) (see Sections III-B5, III-B6 for details).

Over a wide range of PSNR values, we present results for IA estimation in Fig. 5. In Fig. 5, we present results for QEA and QLM. Similarly, we present IF estimation results for QLM, QEA, and VS-LLP in Fig. 6 (x direction only). In Fig. 6(c), we present the results for high frequency ($\varphi_x = \varphi_y = 5\pi/8$) Gaussian amplitude modulated signals. For these results, we applied pre- and postfiltering using 3×3 median filters. Here, we compare QLM, QEA, and the modulation version of VS-LLP (see Section III-B5 for details).

B. Reconstructions Using Natural Images

We present results for natural images from [60]: 38 aerial images, 64 texture images and 44 miscellaneous images (including the standards *Lena* and *Mandrill*). The images were either 256×256 , 512×512 , or 1024×1024 pixels. We present results based on both the MSE and the universal image quality index [61]. We compute the MSE and universal image quality index between the AM-FM reconstructions and the original images.

The image quality index values (Q) are given in Tables VI, VII, and VIII. Fig. 7 shows examples of the reconstructions

for *Lena* using LESH, MULTILES and LESHAL (see Section III-C).

In Fig. 8, we present an analysis of the FM results for *Lena*. The analysis is performed without the lowpass information using a two-scale and a three-scale filterbank. Note that we do not consider pixels with very low IA values to present the most prominent features. To present the most significant components, we focus on pixels with high IA. *Lena* is characterized by a mixture of texture and smooth regions. For *Lena*, we display FM information for IA values that are above the mean.

V. DISCUSSION

In this section, we discuss the results for IA and IF estimation, as well as for general image reconstructions using multiple scales. As we discuss below, VS-LLP provides for significant improvement in IF estimation, while the least-squares AM-FM decompositions can be used to reconstruct general images.

For both IA and IF estimations, we have significant improvements when using the multiscale filterbanks [see Figs. 5 and 6(a) and (b)]. Here, we note that IF estimation does suffer when the instantaneous frequency components are very low. This



Fig. 7. Multiscale AM-FM reconstructions for the *Lena* image. (a) Original image 512×512 pixels. Single-scale filterbank results for: (b) LESH, (c) MULTILES, and (d) LESHAL. Two-scale filterbank results for: (e) LESH, (f) MULTILES, and (g) LESHAL. Three-scale filterbank results for: (h) LESH, (i) MULTILES, and (j) LESHAL.

TABLE VI
IMAGE QUALITY INDEX USING LESH (SECTION III-C1). Q-VALUES ABOVE 0.75 ARE SHOWN IN **BOLD TYPEFACE**

	<i>Single-scale</i>		<i>Two-scale</i>		<i>Three-scale</i>	
	1	5	1	5	1	5
Harmonics						
Aerial	0.7523	0.7523	0.5224	0.5225	0.3255	0.3258
Miscellaneous	0.7664	0.7637	0.5775	0.5764	0.4126	0.4129
Textures	0.8469	0.8469	0.6421	0.6474	0.4063	0.4239

TABLE VII
IMAGE QUALITY INDEX USING MULTILES (SECTION III-C3), SEE TABLE II ALSO. LPF DENOTES THE LOW-PASS FILTER RECONSTRUCTION. L DENOTES THE LOW-FREQUENCY SCALE AM-FM COMPONENT. SIMILARLY, M AND H DENOTE THE MEDIUM- AND HIGH-FREQUENCY SCALE AM-FM COMPONENT. Q-VALUES ABOVE 0.75 ARE SHOWN IN **BOLD TYPEFACE**

Scales	<i>Single-scale</i>		<i>Two-scale</i>		<i>Three-scale</i>	
	LPF1	LPF1+H	LPF2	LPF2+M+H	LPF3	LPF3+L+M+H
Aerial	0.752	0.866	0.522	0.775	0.325	0.779
Miscellaneous	0.763	0.837	0.579	0.747	0.416	0.744
Textures	0.848	0.902	0.650	0.804	0.425	0.814

comes from the requirement that the AM and FM magnitude spectra should remain clearly separated (see Section II-A1 and [62]–[65]).

For IF estimation, VS-LLP is consistently shown to improve estimation over the methods considered here. For single-component signals, without the use of filterbanks, we can see from Fig. 6(a)–(c) that improvements ranged from small up to nearly 20 dB. Similarly, for the same signal, we see significant improvements over regularized AM-FM demodulation (compare results to Table V). From Fig. 6(c), we see dramatic improvements in IF estimation when using VS-LLP with modulation to a lower frequency. Here, modulating to a lower frequency has the effect of “slowing-down” the signal, allowing us to consider IF estimation algorithms with spacings of 1 to 4 pixels. In turn, this “slow-down” helps the local linear phase model become more applicable. We also note that the use of post and pre filtering with a 3×3 median filter has also helped reduce

the noise in this case. Here, recall the advantage of the median filter in that it removes noise without reducing the bandwidth (for single AM-FM components only).

It is also interesting to note the 70 dB improvement over QEA, when the Quadrature signal was provided to both VS-LLP and the QEA (see first column of Table IV). This result suggests that most of the error comes from estimating the Quadrature signal. When the Quadrature signal is provided, the VS-LLP is directly compared to the standard QEA, without accounting for any preprocessing.

We obtained mixed results when using the QLM methods for IF and IA estimations. For example, in Fig. 5, for IA estimation, the QLM gave the best results. However, the IA results are significantly worse (by 3 dB) for the noise-free case that we report in Table III. As we discuss in the methods section, accurate QLM estimation requires that we select appropriate passband bandwidth for a low-pass filter used in the estimation. Here, we

TABLE VIII
IMAGE QUALITY INDEX USING LESHAL (SECTION III-C2). Q-VALUES ABOVE 0.75 ARE SHOWN IN **BOLD TYPEFACE**

	<i>Single-scale</i>		<i>Two-scale</i>		<i>Three-scale</i>	
	LPF1	LPF1+5h*	LPF2	LPF2+5h*	LPF3	LPF3+5h*
Aerial	0.7523	0.8667	0.5225	0.7028	0.3259	0.6110
Miscellaneous	0.7630	0.8355	0.5791	0.6889	0.4161	0.5820
Textures	0.8489	0.9013	0.6504	0.7459	0.4255	0.6683

LPF+5h* = LPF + 5 AM-FM harmonics.

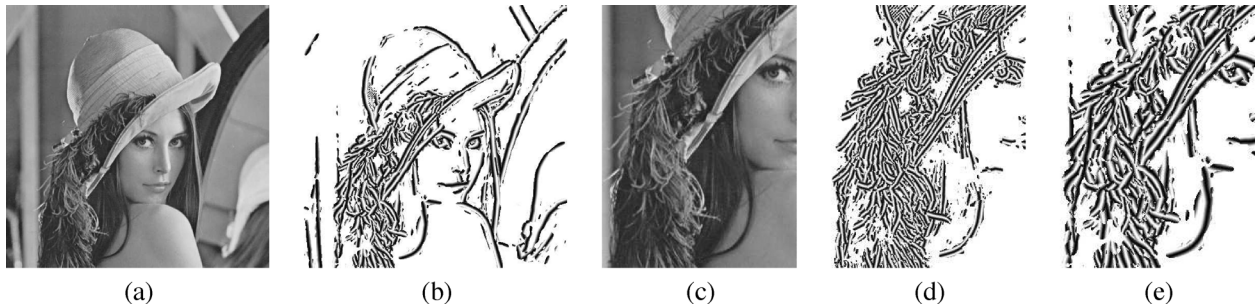


Fig. 8. High amplitude FM Analysis using QEA method for *Lena*. For (b), (d), (g), and (i) we only show the FM component pixels for which the instantaneous amplitude is above the IA mean. For reconstructing the FM image, we plot $\cos \varphi$ for the dominant component, estimated over different scales (excluding estimation over the LPF). (a) Original image. FM analysis in (b) using a three-scale filterbank. Zoom on *Lena*'s hair and feather in (c). FM analysis in (d) using a two-scale filterbank and in (e) using a three-scale filterbank.

did not assume any prior knowledge, and this seems to have had an impact on the estimation. From the plots in Fig. 6, it appears that the IF estimates fall between the QEA and the VS-LLP methods.

To analyze the results for image reconstructions, we refer to Tables VI, VII, and VIII. In all cases, it is important to note the significant role played by the channel filters in each scale. For example, for a single-scale, the spectral support for the LPF is the largest. Similarly, for three-scale reconstructions, the LPF support is the smallest (see Fig. 2). Thus, in considering the quality of the reconstructions, given the fact that most image energy is concentrated around the lower-frequency components, the LPF provides a very significant contribution. We document the contribution of the LPF in all of our tables. This comment also applies to LESHAL reconstructions of Table VI, since the low-frequency components estimated over the LPF will dominate. Here, we note that the “1” columns refer to the use of a single dominant component, while “5” refers to the use of 5 AM-FM harmonics. For LESHAL, the use of AM-FM harmonics did not contribute much to the reconstruction. We attribute this result to the fact that low-frequency components, estimated over the LPF, dominate the reconstruction.

For LESHAL and MULTILES, we do not allow AM-FM demodulation over the LPF. This allows us to measure the contribution of higher-frequency AM-FM components as illustrated in Tables VII and VIII. To recognize the contribution of the AM-FM components, we simply compare the reconstruction quality obtained by the LPF, as opposed to the quality reported in the column that is immediately to its right. The contribution of the AM-FM components comes from the difference between the two columns. After careful examination of the Tables, it is clear that the use of AM-FM components extracted from multiple scales provided for the most significant AM-FM contributions towards the reconstruction. As an example, from the last

column of Table VII, the use of Low, Medium, and High scale AM-FM components (3 total) have elevated the reconstruction quality from below 0.42 to above 0.74.

In Fig. 7, we present examples of the reconstructions for the *Lena* image. In the case of *Lena*, we can see artifacts in her shoulder, even for the best reconstructions. For the worst reconstructions, we see that the images look like a smoothed version of the original. Overall, reconstruction quality was very high for MULTILES (see Table IX). Using three-scales, acceptable reconstruction quality was also attained for all images.

We present results from dominant FM analysis ($\cos \varphi$) in Fig. 8. Fig. 8(g) and (i) shows clearly how the frequency components adapt to *Lena*'s hair and feather.

In what follows, we attempt to provide an interpretation of the accuracy that we obtained in our results. We discuss accuracy in the IF, the IA, and image reconstruction separately.

The success of the VS-LLP algorithm comes from the fact that it adaptively selects accurate IF estimates at every pixel. Here, the basic idea is to look at IF estimates coming from different spacings between the samples, and then select the estimate that also produces the lowest condition number estimate. We have verified experimentally that the IF methods that produced lower condition number estimates have also produced more accurate demodulation results. Overall, this resulted since the numerical stability of the IF estimate is also a function of frequency. It thus makes sense that we would want to consider samples separated by larger distances for lower frequencies as opposed to using smaller distances for higher frequencies.

We attribute the attained accuracy of the multiscale QEA IA estimates to the relatively flat spectral magnitude response of the designed digital filters. The use of nonflat magnitude response will clearly alter the AM-FM component spectrum dramatically. Apparently, it is far more efficient to use digital filters with flat

TABLE IX
MSE AND IMAGE QUALITY INDEX (Q) FOR THE RECONSTRUCTIONS SHOWN IN FIG. 7 AND THE *MANDRILL* IMAGE

Filterbank	Method	<i>Lena</i>		<i>Mandrill</i>	
		MSE	Q	MSE	Q
Single-scale	LESHA	15.5002	0.8336	221.4102	0.7880
	MULTILES	10.2028	0.9000	119.0642	0.8917
	LESHAL	10.1955	0.9001	119.0505	0.8917
Two-scale	LESHA	71.4186	0.6721	439.1018	0.5273
	MULTILES	52.7913	0.8142	220.5814	0.8004
	LESHAL	63.3575	0.7443	279.9986	0.7338
Three-scale	LESHA	121.4774	0.5299	563.9774	0.3224
	MULTILES	48.8083	0.8058	198.5808	0.8104
	LESHAL	90.7965	0.6263	328.6932	0.6612

responses, instead of attempting to compensate for the nonflat response afterwards.

We believe that the use of a robust least-squares approach for combining AM-FM components was an important step that directly led to accurate reconstructions of general images. In other words, the standard use of dominant component analysis does produce AM-FM components that are (generally) far from orthogonal. Our use of a least-squares approach relaxes the assumption that the demodulated AM-FM components should be orthogonal.

VI. CONCLUSIONS AND FUTURE WORK

The first step in developing new AM-FM methods was to design a new multiscale filterbank. The almost flat response in the bandpass frequency of the 1-D filters eliminated errors due to the use of an amplitude correction as in the case of using Gabor filterbanks. The use of these filters in the AM-FM demodulation problem produced big improvements in the IA and IF estimations.

We developed a new method for accurate IF estimation: VS-LLP (see Section III-B4). For noisy signals, VS-LLP produced significantly better results than other methods such as QEA or QLM. We have also developed new QLM methods for IA and IF estimation for digital images.

We developed new methods for reconstructing images based on their IA and IP information. Three least squares methods were presented: MULTILES, LESHA, and LESHAL (see Section III-C). These methods produced good image reconstructions and MULTILES showed that AM-FM components from different scales of the frequency spectrum contain important information that can be used to improve image quality in the reconstruction. Overall, we show that the system provides for accurate reconstructions of general images and show extracted AM-FM component parameters in several cases. Even though the AM-FM reconstructions were promising, our primary focus was on image analysis applications (as demonstrated in the case of *Lena*'s hair and feather).

Clearly, all prior applications that were based on AM-FM demodulation can benefit from using the new filterbanks presented. As an example, Murray reported excellent results from

using the proposed AM-FM methods in retinal image analysis in [66]. We are currently exploring the implementation of AM-FM methods in a dynamically reconfigurable environment on FPGAs. This platform will allow us to explore real-time video processing applications.

REFERENCES

- [1] M. S. Pattichis and A. C. Bovik, "Analyzing image structure by multi-dimensional frequency modulation," *IEEE Trans. Pattern Anal. Mach. Intell.*, vol. 29, no. 5, pp. 753–766, May 2007.
- [2] I. Kokkinos, G. Evangelopoulos, and P. Maragos, "Texture analysis and segmentation using modulation features, generative models, and weighted curve evolution," *IEEE Trans. Pattern Anal. Mach. Intell.*, vol. 31, no. 1, pp. 142–157, Jan. 2009.
- [3] J. F. Kaiser, "On a simple algorithm to calculate the 'energy' of a signal," in *Proc. IEEE Conf. Acoustics, Speech, and Signal Processing*, Albuquerque, NM, Apr. 1990, pp. 381–384.
- [4] P. Maragos, J. F. Kaiser, and T. F. Quatieri, "On amplitude and frequency demodulation using energy operators," *IEEE Trans. Signal Process.*, vol. 41, no. 4, pp. 1532–1550, Apr. 1993.
- [5] P. Maragos, J. F. Kaiser, and T. F. Quatieri, "Energy separation in signal modulations with applications to speech analysis," *IEEE Trans. Signal Process.*, vol. 41, no. 10, pp. 3024–3051, Oct. 1993.
- [6] A. Bovik, P. Maragos, and T. Quatieri, "AM-FM energy detection and separation in noise using multiband energy operators," *IEEE Trans. Signal Process.*, vol. ASSP-41, no. 12, pp. 3245–3265, Dec. 1993.
- [7] G. Girolami and D. Vakman, "Instantaneous frequency estimation and measurement: A Quasi-local method," *Meas. Sci. Technol.*, vol. 13, pp. 909–917, Jun. 2002.
- [8] B. Santhanam and P. Maragos, "Multicomponent AM-FM demodulation via periodicity-based algebraic separation and energy-based demodulation," *IEEE Trans. Commun.*, vol. 48, no. 3, pp. 473–490, Mar. 2000.
- [9] R. A. Baxter and T. F. Quatieri, "Shunting networks for multi-band AM-FM decomposition," in *Proc. IEEE Workshop on Applications of Signal Processing to Audio and Acoustics*, Oct. 1999, pp. 227–230.
- [10] M. R. Morelande and A. M. Zoubir, "Model selection of random amplitude polynomial phase signals," *IEEE Trans. Signal Process.*, vol. 50, no. 3, pp. 578–589, Mar. 2002.
- [11] D. Dimitriadis and P. Maragos, "An improved energy demodulation algorithm using splines," presented at the IEEE Conf. Acoustics, Speech, and Signal Processing, May 2001.
- [12] B. Santhanam, "Generalized energy demodulation for large frequency deviations and wideband signals," *IEEE Signal Process. Lett.*, vol. 11, no. 3, pp. 341–344, Mar. 2004.
- [13] G. Evangelopoulos and P. Maragos, "Multiband modulation energy tracking for noisy speech detection," *IEEE Trans. Audio, Speech, Lang. Process.*, vol. 14, no. 6, pp. 2024–2038, Nov. 2006.
- [14] D. Dimitriadis and P. Maragos, "Continuous energy demodulation methods and application to speech analysis," *Speech Commun.*, vol. 48, no. 7, pp. 819–837, Jul. 2006.

- [15] D. Dimitriadis and P. Maragos, "Robust energy demodulation based on continuous models with application to speech recognition," presented at the European Conf. Speech Communication Technology, Sept. 2003.
- [16] S. Gazor and R. R. Far, "Adaptive maximum windowed likelihood multicomponent AM-FM signal decomposition," *IEEE Trans. Audio, Speech, Lang. Process.*, vol. 14, pp. 479–491, 2006.
- [17] F. Gianfelici, G. Biagetti, P. Crippa, and C. Turchetti, "Multicomponent AM-FM representations: An asymptotically exact approach," *IEEE Trans. Audio, Speech, Lang. Process.*, vol. 15, pp. 823–837, 2007.
- [18] B. J. Super and A. C. Bovik, "Shape from texture using local spectral moments," *IEEE Trans. Pattern Anal. Mach. Intell.*, vol. 17, no. 4, pp. 333–343, Apr. 1995.
- [19] M. Pattichis, G. Panayi, A. Bovik, and H. Shun-Pin, "Fingerprint classification using an AM-FM model," *IEEE Trans. Image Process.*, vol. 10, no. 6, pp. 951–954, Jun. 2001.
- [20] J. Havlicek, J. Tang, S. Acton, R. Antonucci, and F. Quandji, "Modulation domain texture retrieval for CBIR in digital libraries," presented at the 37th IEEE Asilomar Conf. Signals, Systems and Computers, Pacific Grove, CA, Nov. 2003.
- [21] M. Pattichis, C. Pattichis, M. Avraam, A. Bovik, and K. Kyriakou, "AM-FM texture segmentation in electron microscopic muscle imaging," *IEEE Trans. Med. Imag.*, vol. 19, no. 12, pp. 1253–1258, Dec. 2000.
- [22] T. Yap, J. Havlicek, and V. DeBrunner, "Bayesian segmentation of AM-FM texture images," in *Proc. 35th IEEE Asilomar Conf. Signals, Systems and Computers*, Pacific Grove, CA, Nov. 2001, vol. 2, pp. 1156–1160.
- [23] N. Ray, J. Havlicek, S. T. Acton, and M. S. Pattichis, "Active contour segmentation guided by AM-FM dominant component analysis," in *Proc. IEEE Int. Conf. Image Processing*, 2001, pp. 78–81.
- [24] S. T. Acton, D. P. Mukherjee, J. P. Havlicek, and A. C. Bovik, "Oriented texture completion by AM-FM reaction-diffusion," *IEEE Trans. Image Process.*, vol. 10, no. 6, pp. 885–896, Jun. 2001.
- [25] J. Havlicek, P. Tay, and A. Bovik, *Handbook of Image and Video Processing*. New York: Elsevier, 2005, pp. 377–395, ch. AM-FM Image Models: Fundamental Techniques and Emerging Trends.
- [26] P. Rodriguez, V. M. Pattichis, and M. Goens, "M-mode echocardiography image and video segmentation based on AM-FM demodulation techniques," in *Proc. 25th Int. Conf. IEEE Engineering in Medicine and Biology Society*, Sep. 2003, vol. 2, pp. 1176–1179.
- [27] D. J. Fleet and A. D. Jepson, "Computation of component image velocity from local phase information," *Int. J. Comput. Vis.*, vol. 5, no. 1, pp. 77–104, 1990.
- [28] V. Murray, S. Murillo, M. Pattichis, C. Loizou, C. Pattichis, E. Kyriacou, and A. Nicolaidis, "An AM-FM model for motion estimation in atherosclerotic plaque videos," in *Proc. 41st IEEE Asilomar Conf. Signals, Systems, Computers*, 2007, pp. 746–750.
- [29] V. Murray and M. S. Pattichis, "AM-FM demodulation methods for reconstruction, analysis and motion estimation in video signals," in *Proc. IEEE Southwest Symp. Image Analysis, and Interpretation*, Mar. 2008, pp. 17–20.
- [30] M. S. Pattichis, A. C. Bovik, J. W. Havlicek, and N. D. Sidiropoulos, "Multidimensional orthogonal FM transforms," *IEEE Trans. Image Process.*, vol. 10, no. 3, pp. 448–464, Mar. 2001.
- [31] J. P. Havlicek and A. C. Bovik, "Multi-component AM-FM image models and wavelet-based demodulation with component tracking," in *Proc. IEEE Int. Conf. Image Processing*, 1994, pp. 41–45 [Online]. Available: citeseer.ist.psu.edu/531852.html
- [32] J. P. Havlicek, D. S. Harding, and A. C. Bovik, "The multi-component AM-FM image representation," *IEEE Trans. Image Process.*, vol. 5, no. 6, pp. 1094–1100, Jun. 1996.
- [33] J. P. Havlicek, D. S. Harding, and A. C. Bovik, "Computation of the Multi-Component AM-FM Image Representation," The Univ. Texas at Austin, Tech. Rep., 1996.
- [34] J. P. Havlicek, D. S. Harding, and A. C. Bovik, "Reconstruction from the multi-component AM-FM image representation," in *Proc. IEEE Int. Conf. Image Processing*, Oct. 1995, vol. 2, pp. 280–283.
- [35] V. Murray, P. V. Rodriguez, and M. S. Pattichis, "Robust multiscale AM-FM demodulation of digital images," in *Proc. IEEE Int. Conf. Image Processing*, Oct. 2007, vol. 1, pp. 465–468.
- [36] R. A. Sivley and J. P. Havlicek, "Perfect reconstruction AM-FM image models," in *Proc. IEEE Int. Conf. Image Processing*, Oct. 2006, pp. 2125–2128.
- [37] K. Suri and J. P. Havlicek, "Phase algorithm for blocking artifact reduction in reconstructions from analysis-only AM-FM models," in *Proc. IEEE Southwest Symp. Image Analysis and Interpretation*, 2006, pp. 6–10.
- [38] J. P. Havlicek, D. S. Harding, and A. C. Bovik, "Multi-component signal demodulation and reconstruction using AM-FM modulation models," in *Proc. IEEE Workshop on Nonlinear Signal and Image Processing*, Jun. 1995, pp. 41–45.
- [39] R. A. Sivley and J. P. Havlicek, "A spline-based framework for perfect reconstruction AM-FM models," in *Proc. IEEE Southwest Symp. Image Analysis and Interpretation*, 2006, pp. 198–202.
- [40] J. P. Havlicek, "AM-FM Image Models" Ph.D. dissertation, The Univ. Texas at Austin, , 1996 [Online]. Available: <http://hotnsour.ou.edu/joebob/PdfPubs/JPHavlicekDiss.pdf>
- [41] K. G. Larkin, D. J. Bone, and M. A. Oldfield, "Natural demodulation of two-dimensional fringe patterns. I. General background of the spiral phase quadrature transform," *J. Opt. Soc. Amer. A: Opt., Image Sci., Vis.*, vol. 18, no. 8, pp. 1862–1870, Aug. 2001.
- [42] K. G. Larkin, "Natural demodulation of two-dimensional fringe patterns. II. Stationary phase analysis of the spiral phase quadrature transform," *J. Opt. Soc. Amer. A: Opt., Image Sci., Vis.*, vol. 18, no. 8, pp. 1871–1881, Aug. 2001.
- [43] M. Felsberg and G. Sommer, "The monogenic signal," *IEEE Trans. Signal Process.*, vol. 49, no. 12, pp. 3136–3144, Dec. 2001.
- [44] S. L. Hahn, The Analytic, Quaternionic and Monogenic 2-D Complex Delta Distributions Warsaw Univ. Technology, Inst. Radioelectronics, Nowowiejska, Rep. 3, Apr. 2002.
- [45] T. Bülrow and G. Sommer, "Hypercomplex signals—A novel extension of the analytic signal to the multidimensional case," *IEEE Trans. Signal Process.*, vol. 49, no. 11, pp. 2844–2852, Nov. 2001.
- [46] U. Köthe and M. Felsberg, "Riesz-transforms vs. derivatives: On the relationship between the boundary tensor and the energy tensor," in *Scale Space and PDE Methods in Computer Vision*, R. Kimmel, N. Sochen, and J. Weickert, Eds. New York: Springer, 2005, vol. 3459, pp. 179–191, ser. LNCS.
- [47] D. Vakman, "On the analytic signal, the teager-kaiser energy algorithm, and other methods for defining amplitude and frequency," *IEEE Trans. Signal Process.*, vol. 44, no. 4, pp. 791–797, Apr. 1996.
- [48] D. Vakman, *Signals, Oscillations, and Waves: A Modern Approach*. Boston, MA: Artech House, 1998.
- [49] J. Havlicek and A. Bovik, *Handbook of Image and Video Processing*, ser. Communications, Networking, and Multimedia. San Diego, CA: Academic Press, 2000, pp. 305–316, ch. Image Modulation Models.
- [50] M. Pattichis, J. Havlicek, S. Acton, and A. Bovik, *Advances in Image Processing and Understanding: A Festschrift for Thomas S. Huang*, ser. Machine Perception and Artificial Intelligence. Singapore: World Scientific, 2002, vol. 52, pp. 277–305, ch. Multidimensional AM-FM Models with Image Processing Applications.
- [51] T. Strom, "On amplitude-weighted instantaneous frequencies," *IEEE Trans. Acoust., Speech, Signal Process.*, vol. ASSP-25, no. 4, pp. 351–353, Aug. 1977.
- [52] J. P. Havlicek, D. S. Harding, and A. C. Bovik, "Multidimensional quasi-eigenfunction approximations and multicomponent AM-FM models," *IEEE Trans. Image Process.*, vol. 9, no. 2, pp. 227–242, Feb. 2000.
- [53] S. Hahn, "Multidimensional complex signals with single-orthant spectra," *Proc. IEEE*, vol. 80, no. 8, pp. 1287–1300, Aug. 1992.
- [54] L. Cohen, *Time-Frequency Analysis*, ser. Prentice-Hall Signal Processing, A. V. Oppenheim, Ed. Englewood Cliffs, NJ: Prentice-Hall, 1995.
- [55] S. D. Conte and C. de Boor, *Elementary Numerical Analysis: An Algorithmic Approach*. New York: McGraw-Hill, 1980.
- [56] D. Kincaid and W. Cheney, *Numerical Analysis Mathematics of Scientific Computing*. Pacific Grove, CA: Brooks/Cole, 1991.
- [57] A. Bovik, N. Gopal, T. Emmoth, and A. Restrepo, "Localized measurement of emergent image frequencies by gabor wavelets," *IEEE Trans. Inf. Theory*, vol. 38, no. 2, pp. 691–712, Mar. 1992.
- [58] J. W. Demmel, *Applied Numerical Linear Algebra*. Philadelphia, PA: SIAM, 1997, pp. 105–117, ch. Linear Least Square Problems.
- [59] M. S. Pattichis, "AM-FM Transforms With Applications," Ph.D. dissertation, Univ. Texas, Austin, 1998.
- [60] The USC-SIPI Image Database Signal and I. P. I. of the University of Southern California [Online]. Available: <http://sipi.usc.edu/database/>

- [61] Z. Wang and A. C. Bovik, "A universal image quality index," *IEEE Signal Process. Lett.*, vol. 9, no. 3, pp. 81–84, Mar. 2002.
- [62] A. Nuttall and E. Bedrosian, "On the quadrature approximation to the hilbert transform of modulated signals," *Proc. IEEE*, vol. 54, no. 10, pp. 1458–1459, Oct. 1966.
- [63] H. Stark, "An extension of the Hilbert transform product theorem," *Proc. IEEE*, vol. 59, no. 9, pp. 1359–1360, Sep. 1971.
- [64] E. Bedrosian, "A product theorem for Hilbert transforms," *Proc. IEEE*, vol. 51, no. 5, pp. 868–869, May 1963.
- [65] E. Bedrosian and H. Stark, "Comments on an extension of the hilbert transform product theorem," *Proc. IEEE*, vol. 60, no. 2, pp. 228–229, Feb. 1972.
- [66] AM-FM Methods for Image and Video Processing, Ph.D. dissertation, Univ. New Mexico, Sep. 2008, Victor Manuel Murray Herrera.



Víctor Murray (M'01) received the B.S. degree in electrical engineering from the Pontificia Universidad Católica del Perú (PUCP), Lima, Perú, in 2003, and the M.S. and Ph.D. degrees in electrical engineering from the University of New Mexico (UNM), Albuquerque, in 2005 and 2008, respectively.

He is a Research Assistant Professor in the Electrical and Computer Engineering Department (ECE), UNM, where he is developing reconfigurable architectures using FPGAs for the Air Force Research Lab and developing methods and algorithms in medical

imaging for detecting diseases in human eyes for VisionQuest Biomedical, Albuquerque. His research interests include AM-FM demodulation methods, digital image and video processing, and hardware design using VHDL and FPGAs.



Paul Rodríguez received the B.Sc. degree in electrical engineering from the Pontificia Universidad Católica del Perú, Lima, Peru, in 1997, and the M.Sc. and Ph.D. degrees in electrical engineering from the University of New Mexico, Albuquerque, in 2003 and 2005, respectively.

He spent two years as a postdoctoral researcher at Los Alamos National Laboratory and is currently an Associate Professor with the Department of Electrical Engineering at Pontificia Universidad Católica del Perú. His research interests include AM-FM models, SIMD algorithms, adaptive signal decompositions, and inverse problems in signal and image processing.



Marios S. Pattichis (M'99–SM'06) received the B.Sc. (high honors and special honors) degree in computer sciences and the B.A. (high honors) degree in mathematics in 1991, the M.S. degree in electrical engineering in 1993, and the Ph.D. degree in computer engineering in 1998 from the University of Texas at Austin.

He is currently an Associate Professor in the Department of Electrical and Computer Engineering (ECE), University of New Mexico (UNM), Albuquerque, where he is also an Associate Professor in the Department of Radiology. His current research interests include digital image, and video processing and communications, dynamically reconfigurable computer architectures, and biomedical and space image processing applications.

Dr. Pattichis is an Associate Editor of the IEEE TRANSACTIONS ON INDUSTRIAL INFORMATICS and an Associate Editor of *Pattern Recognition*. He was the General Chair of the 2008 IEEE Southwest Symposium on Image Analysis and Interpretation. At UNM, he received the 2004 ECE Distinguished Teaching Award and the 2006 School of Engineering Harrison Faculty Recognition Award.